広島大学学術情報リポジトリ
Hiroshima University Institutional Repository

Title	Azimuthal correlations of electrons from heavy-flavor decay with hadrons in p+p and Au+Au collisions at $\sqrt{s_{NN}}$ = 200 GeV
Auther(s)	PHENIX Collaboration, ; Haruna, K.; Homma, Kensuke; Horaguchi, T.; Kijima, K. M.; Nakamiya, Y.; Nakamura, T.; Ouchida, M.; Shigaki, Kenta; Sugitate, Toru; Torii, H.; Tsuchimoto, Y.; Watanabe, D.; Yamaura, K.
Citation	Physical Review C , 83 (4) : 044912-1 - 044912-16
Issue Date	2011-04-26
DOI	10.1103/PhysRevC.83.044912
Self DOI	
URL	http://ir.lib.hiroshima-u.ac.jp/00045820
Right	Copyright (c) 2011 American Physical Society
Relation	

Hiroshima University Institutional Repository

Azimuthal correlations of electrons from heavy-flavor decay with hadrons in $p+p$ and Au+Au collisions at $\sqrt{s_{NN}} = 200$ GeV

A. Adare,[12] S. Afanasiev,[28] C. Aidala,[41] N. N. Ajitanand,[58] Y. Akiba,[52,53] H. Al-Bataineh,[47] J. Alexander,[58] K. Aoki,[34,52]
L. Aphecetche,[60] Y. Aramaki,[11] J. Asai,[52] E. T. Atomssa,[35] R. Averbeck,[59] T. C. Awes,[48] B. Azmoun,[6] V. Babintsev,[23] M. Bai,[5]
G. Baksay,[19] L. Baksay,[19] A. Baldisseri,[15] K. N. Barish,[7] P. D. Barnes,[37] B. Bassalleck,[46] A. T. Basye,[1] S. Bathe,[7] S. Batsouli,[48]
V. Baublis,[51] C. Baumann,[42] A. Bazilevsky,[6] S. Belikov,[6,*] R. Belmont,[64] R. Bennett,[59] A. Berdnikov,[55] Y. Berdnikov,[55]
A. A. Bickley,[12] J. G. Boissevain,[37] J. S. Bok,[67] H. Borel,[15] K. Boyle,[59] M. L. Brooks,[37] H. Buesching,[6] V. Bumazhnov,[23]
G. Bunce,[6,53] S. Butsyk,[37] C. M. Camacho,[37] S. Campbell,[59] B. S. Chang,[67] W. C. Chang,[2] J.-L. Charvet,[15] C.-H. Chen,[59]
S. Chernichenko,[23] C. Y. Chi,[13] M. Chiu,[6,24] I. J. Choi,[67] R. K. Choudhury,[4] P. Christiansen,[39] T. Chujo,[63] P. Chung,[58]
A. Churyn,[23] O. Chvala,[7] V. Cianciolo,[48] Z. Citron,[59] B. A. Cole,[13] M. Connors,[59] P. Constantin,[37] M. Csanád,[17] T. Csörgő,[31]
T. Dahms,[59] S. Dairaku,[34,52] I. Danchev,[64] K. Das,[20] A. Datta,[41] G. David,[6] A. Denisov,[23] D. d'Enterria,[35] A. Deshpande,[53,59]
E. J. Desmond,[6] O. Dietzsch,[56] A. Dion,[59] M. Donadelli,[56] O. Drapier,[35] A. Drees,[59] K. A. Drees,[5] A. K. Dubey,[66]
J. M. Durham,[59] A. Durum,[23] D. Dutta,[4] V. Dzhordzhadze,[7] S. Edwards,[20] Y. V. Efremenko,[48] F. Ellinghaus,[12] T. Engelmore,[13]
A. Enokizono,[36] H. En'yo,[52,53] S. Esumi,[63] K. O. Eyser,[7] B. Fadem,[43] D. E. Fields,[46,53] M. Finger Jr.,[8] M. Finger,[8]
F. Fleuret,[35] S. L. Fokin,[33] Z. Fraenkel,[66,*] J. E. Frantz,[59] A. Franz,[6] A. D. Frawley,[20] K. Fujiwara,[52] Y. Fukao,[34,52]
T. Fusayasu,[45] I. Garishvili,[61] A. Glenn,[12] H. Gong,[59] M. Gonin,[35] J. Gosset,[15] Y. Goto,[52,53] R. Granier de Cassagnac,[35]
N. Grau,[13] S. V. Greene,[64] M. Grosse Perdekamp,[24,53] T. Gunji,[11] H.-Å. Gustafsson,[39,*] A. Hadj Henni,[60] J. S. Haggerty,[6]
K. I. Hahn,[18] H. Hamagaki,[11] J. Hamblen,[61] J. Hanks,[13] R. Han,[50] E. P. Hartouni,[36] K. Haruna,[22] E. Haslum,[39] R. Hayano,[11]
M. Heffner,[36] T. K. Hemmick,[59] T. Hester,[7] X. He,[21] J. C. Hill,[27] M. Hohlmann,[19] W. Holzmann,[13,58] K. Homma,[22] B. Hong,[32]
T. Horaguchi,[11,22,52,62] D. Hornback,[61] S. Huang,[64] T. Ichihara,[52,53] R. Ichimiya,[52] J. Ide,[43] H. Iinuma,[34,52] Y. Ikeda,[63]
K. Imai,[34,52] J. Imrek,[16] M. Inaba,[63] D. Isenhower,[1] M. Ishihara,[52] T. Isobe,[11] M. Issah,[58,64] A. Isupov,[28] D. Ivanischev,[51]
B. V. Jacak,[59,†] J. Jia,[6,13,58] J. Jin,[13] B. M. Johnson,[6] K. S. Joo,[44] D. Jouan,[49] D. S. Jumper,[1] F. Kajihara,[11] S. Kametani,[52]
N. Kamihara,[53] J. Kamin,[59] J. H. Kang,[67] J. Kapustinsky,[37] K. Karatsu,[34] D. Kawall,[41,53] M. Kawashima,[54,52] A. V. Kazantsev,[33]
T. Kempel,[27] A. Khanzadeev,[51] K. M. Kijima,[22] J. Kikuchi,[65] B. I. Kim,[32] D. H. Kim,[44] D. J. Kim,[29,67] E. J. Kim,[9] E. Kim,[57]
S. H. Kim,[67] Y. J. Kim,[24] E. Kinney,[12] K. Kiriluk,[12] Á. Kiss,[17] E. Kistenev,[6] J. Klay,[36] C. Klein-Boesing,[42] L. Kochenda,[51]
B. Komkov,[51] M. Konno,[63] J. Koster,[24] D. Kotchetkov,[46] A. Kozlov,[66] A. Král,[14] A. Kravitz,[13] G. J. Kunde,[37] K. Kurita,[54,52]
M. Kurosawa,[52] M. J. Kweon,[32] Y. Kwon,[61,67] G. S. Kyle,[47] R. Lacey,[58] Y. S. Lai,[13] J. G. Lajoie,[27] D. Layton,[24] A. Lebedev,[27]
D. M. Lee,[37] J. Lee,[18] K. B. Lee,[32] K. Lee,[57] K. S. Lee,[32] T. Lee,[57] M. J. Leitch,[37] M. A. L. Leite,[56] E. Leitner,[64] B. Lenzi,[56]
P. Liebing,[53] L. A. Linden Levy,[12] T. Liška,[14] A. Litvinenko,[28] H. Liu,[37,47] M. X. Liu,[37] X. Li,[10] B. Love,[64] R. Luechtenborg,[42]
D. Lynch,[6] C. F. Maguire,[64] Y. I. Makdisi,[5] A. Malakhov,[28] M. D. Malik,[46] V. I. Manko,[33] E. Mannel,[13] Y. Mao,[50,52]
L. Mašek,[8,26] H. Masui,[63] F. Matathias,[13] M. McCumber,[59] P. L. McGaughey,[37] N. Means,[59] B. Meredith,[24] Y. Miake,[63]
A. C. Mignerey,[40] P. Mikeš,[8,26] K. Miki,[63] A. Milov,[6] M. Mishra,[3] J. T. Mitchell,[6] A. K. Mohanty,[4] Y. Morino,[11] A. Morreale,[7]
D. P. Morrison,[6] T. V. Moukhanova,[33] D. Mukhopadhyay,[64] J. Murata,[54,52] S. Nagamiya,[30] J. L. Nagle,[12] M. Naglis,[66]
M. I. Nagy,[17] I. Nakagawa,[52,53] Y. Nakamiya,[22] T. Nakamura,[22,30] K. Nakano,[52,62] J. Newby,[36] M. Nguyen,[59] T. Niita,[63]
R. Nouicer,[6] A. S. Nyanin,[33] E. O'Brien,[6] S. X. Oda,[11] C. A. Ogilvie,[27] K. Okada,[53] M. Oka,[63] Y. Onuki,[52] A. Oskarsson,[39]
M. Ouchida,[22] K. Ozawa,[11] R. Pak,[6] A. P. T. Palounek,[37] V. Pantuev,[25,59] V. Papavassiliou,[47] I. H. Park,[18] J. Park,[57] S. K. Park,[32]
W. J. Park,[32] S. F. Pate,[47] H. Pei,[27] J.-C. Peng,[24] H. Pereira,[15] V. Peresedov,[28] D.Yu. Peressounko,[33] C. Pinkenburg,[6]
R. P. Pisani,[6] M. Proissl,[59] M. L. Purschke,[6] A. K. Purwar,[37] H. Qu,[21] J. Rak,[29,46] A. Rakotozafindrabe,[35] I. Ravinovich,[66]
K. F. Read,[48,61] S. Rembeczki,[19] K. Reygers,[42] V. Riabov,[51] Y. Riabov,[51] E. Richardson,[40] D. Roach,[64] G. Roche,[38]
S. D. Rolnick,[7] M. Rosati,[27] C. A. Rosen,[12] S. S. E. Rosendahl,[39] P. Rosnet,[38] P. Rukoyatkin,[28] P. Ružička,[26] V. L. Rykov,[52]
B. Sahlmueller,[42] N. Saito,[30,34,52,53] T. Sakaguchi,[6] S. Sakai,[63] K. Sakashita,[52,62] V. Samsonov,[51] S. Sano,[11,65] T. Sato,[63]
S. Sawada,[30] K. Sedgwick,[7] J. Seele,[12] R. Seidl,[24] A.Yu. Semenov,[27] V. Semenov,[23] R. Seto,[7] D. Sharma,[66] I. Shein,[23]
T.-A. Shibata,[52,62] K. Shigaki,[22] M. Shimomura,[63] K. Shoji,[34,52] P. Shukla,[4] A. Sickles,[6] C. L. Silva,[56] D. Silvermyr,[48]
C. Silvestre,[15] K. S. Sim,[32] B. K. Singh,[3] C. P. Singh,[3] V. Singh,[3] M. Slunečka,[8] A. Soldatov,[23] R. A. Soltz,[36]
W. E. Sondheim,[37] S. P. Sorensen,[61] I. V. Sourikova,[6] N. A. Sparks,[1] F. Staley,[15] P. W. Stankus,[48] E. Stenlund,[39] M. Stepanov,[47]
A. Ster,[31] S. P. Stoll,[6] T. Sugitate,[22] C. Suire,[49] A. Sukhanov,[6] J. Sun,[59] J. Sziklai,[31] E. M. Takagui,[56] A. Taketani,[52,53]
R. Tanabe,[63] Y. Tanaka,[45] K. Tanida,[34,52,53,57] M. J. Tannenbaum,[6] S. Tarafdar,[3] A. Taranenko,[58] P. Tarján,[16] H. Themann,[59]
T. L. Thomas,[46] M. Togawa,[34,52] A. Toia,[59] L. Tomášek,[26] Y. Tomita,[63] H. Torii,[22,52] R. S. Towell,[1] V-N. Tram,[35] I. Tserruya,[66]
Y. Tsuchimoto,[22] C. Vale,[6,27] H. Valle,[64] H. W. van Hecke,[37] E. Vazquez-Zambrano,[13] A. Veicht,[24] J. Velkovska,[64]
R. Vértesi,[16,31] A. A. Vinogradov,[33] M. Virius,[14] V. Vrba,[26] E. Vznuzdaev,[51] X. R. Wang,[47] D. Watanabe,[22] K. Watanabe,[63]
Y. Watanabe,[52,53] F. Wei,[27] R. Wei,[58] J. Wessels,[42] S. N. White,[6] D. Winter,[13] J. P. Wood,[1] C. L. Woody,[6] R. M. Wright,[1]
M. Wysocki,[12] W. Xie,[53] Y. L. Yamaguchi,[11,65] K. Yamaura,[22] R. Yang,[24] A. Yanovich,[23] J. Ying,[21] S. Yokkaichi,[52,53]
G. R. Young,[48] I. Younus,[46] Z. You,[50] I. E. Yushmanov,[33] W. A. Zajc,[13] O. Zaudtke,[42] C. Zhang,[48] S. Zhou,[10] and L. Zolin[28]

(PHENIX Collaboration)

[1]*Abilene Christian University, Abilene, Texas 79699, USA*

[2]*Institute of Physics, Academia Sinica, Taipei 11529, Taiwan*

[3]*Department of Physics, Banaras Hindu University, Varanasi 221005, India*

[4]*Bhabha Atomic Research Centre, Bombay 400 085, India*

[5]*Collider Accelerator Department, Brookhaven National Laboratory, Upton, New York 11973-5000, USA*

[6]*Physics Department, Brookhaven National Laboratory, Upton, New York 11973-5000, USA*

[7]*University of California—Riverside, Riverside, California 92521, USA*

[8]*Charles University, Ovocný trh 5, Praha 1, 116 36, Prague, Czech Republic*

[9]*Chonbuk National University, Jeonju, 561-756, Korea*

[10]*Science and Technology on Nuclear Data Laboratory, China Institute of Atomic Energy, Beijing, People's Republic of China*

[11]*Center for Nuclear Study, Graduate School of Science, University of Tokyo, 7-3-1 Hongo, Bunkyo, Tokyo 113-0033, Japan*

[12]*University of Colorado, Boulder, Colorado 80309, USA*

[13]*Columbia University, New York, New York 10027 and Nevis Laboratories, Irvington, New York 10533, USA*

[14]*Czech Technical University, Zikova 4, 166 36 Prague 6, Czech Republic*

[15]*Dapnia, CEA Saclay, F-91191, Gif-sur-Yvette, France*

[16]*Debrecen University, H-4010 Debrecen, Egyetem tér 1, Hungary*

[17]*ELTE, Eötvös Loránd University, H - 1117 Budapest, Pázmány P. s. 1/A, Hungary*

[18]*Ewha Womans University, Seoul 120-750, Korea*

[19]*Florida Institute of Technology, Melbourne, Florida 32901, USA*

[20]*Florida State University, Tallahassee, Florida 32306, USA*

[21]*Georgia State University, Atlanta, Georgia 30303, USA*

[22]*Hiroshima University, Kagamiyama, Higashi-Hiroshima 739-8526, Japan*

[23]*IHEP Protvino, State Research Center of Russian Federation, Institute for High Energy Physics, Protvino, 142281, Russia*

[24]*University of Illinois at Urbana-Champaign, Urbana, Illinois 61801, USA*

[25]*Institute for Nuclear Research of the Russian Academy of Sciences, prospekt 60-letiya Oktyabrya 7a, Moscow 117312, Russia*

[26]*Institute of Physics, Academy of Sciences of the Czech Republic, Na Slovance 2, 182 21 Prague 8, Czech Republic*

[27]*Iowa State University, Ames, Iowa 50011, USA*

[28]*Joint Institute for Nuclear Research, 141980 Dubna, Moscow Region, Russia*

[29]*Helsinki Institute of Physics and University of Jyväskylä, P.O.Box 35, FI-40014 Jyväskylä, Finland*

[30]*KEK, High Energy Accelerator Research Organization, Tsukuba, Ibaraki 305-0801, Japan*

[31]*KFKI Research Institute for Particle and Nuclear Physics of the Hungarian Academy of Sciences (MTA KFKI RMKI), Budapest 114,
P. O. Box 49, H-1525 Budapest, Hungary*

[32]*Korea University, Seoul, 136-701, Korea*

[33]*Russian Research Center "Kurchatov Institute," Moscow, Russia*

[34]*Kyoto University, Kyoto 606-8502, Japan*

[35]*Laboratoire Leprince-Ringuet, Ecole Polytechnique, CNRS-IN2P3, Route de Saclay, F-91128, Palaiseau, France*

[36]*Lawrence Livermore National Laboratory, Livermore, California 94550, USA*

[37]*Los Alamos National Laboratory, Los Alamos, New Mexico 87545, USA*

[38]*LPC, Université Blaise Pascal, CNRS-IN2P3, Clermont-Fd, F-63177 Aubiere Cedex, France*

[39]*Department of Physics, Lund University, Box 118, SE-221 00 Lund, Sweden*

[40]*University of Maryland, College Park, Maryland 20742, USA*

[41]*Department of Physics, University of Massachusetts, Amherst, Massachusetts 01003-9337, USA*

[42]*Institut fur Kernphysik, University of Muenster, D-48149 Muenster, Germany*

[43]*Muhlenberg College, Allentown, Pennsylvania 18104-5586, USA*

[44]*Myongji University, Yongin, Kyonggido 449-728, Korea*

[45]*Nagasaki Institute of Applied Science, Nagasaki-shi, Nagasaki 851-0193, Japan*

[46]*University of New Mexico, Albuquerque, New Mexico 87131, USA*

[47]*New Mexico State University, Las Cruces, New Mexico 88003, USA*

[48]*Oak Ridge National Laboratory, Oak Ridge, Tennessee 37831, USA*

[49]*IPN-Orsay, Universite Paris Sud, CNRS-IN2P3, BP1, F-91406, Orsay, France*

[50]*Peking University, Beijing, People's Republic of China*

[51]*PNPI, Petersburg Nuclear Physics Institute, Gatchina, Leningrad region, 188300, Russia*

[52]*RIKEN Nishina Center for Accelerator-Based Science, Wako, Saitama 351-0198, Japan*

[53]*RIKEN BNL Research Center, Brookhaven National Laboratory, Upton, New York 11973-5000, USA*

[54]*Physics Department, Rikkyo University, 3-34-1 Nishi-Ikebukuro, Toshima, Tokyo 171-8501, Japan*

[55]*Saint Petersburg State Polytechnic University, St. Petersburg, Russia*

[56]*Universidade de São Paulo, Instituto de Física, Caixa Postal 66318, São Paulo CEP05315-970, Brazil*

[57]*Seoul National University, Seoul, Korea*

[58]*Chemistry Department, Stony Brook University, SUNY, Stony Brook, New York 11794-3400, USA*

[59]*Department of Physics and Astronomy, Stony Brook University, SUNY, Stony Brook, New York 11794-3400, USA*

[60]*SUBATECH, Ecole des Mines de Nantes, CNRS-IN2P3, Université de Nantes, BP 20722, F-44307 Nantes, France*

[61]*University of Tennessee, Knoxville, Tennessee 37996, USA*

[62]*Department of Physics, Tokyo Institute of Technology, Oh-okayama, Meguro, Tokyo 152-8551, Japan*

[63]*Institute of Physics, University of Tsukuba, Tsukuba, Ibaraki 305, Japan*

[64]*Vanderbilt University, Nashville, Tennessee 37235, USA*

[65]*Waseda University, Advanced Research Institute for Science and Engineering, 17 Kikui-cho, Shinjuku-ku, Tokyo 162-0044, Japan*

[66]*Weizmann Institute, Rehovot 76100, Israel*

[67]*Yonsei University, IPAP, Seoul 120-749, Korea*

Measurements of electrons from the decay of open-heavy-flavor mesons have shown that the yields are suppressed in Au+Au collisions compared to expectations from binary-scaled $p+p$ collisions. These measurements indicate that charm and bottom quarks interact with the hot dense matter produced in heavy-ion collisions much more than expected. Here we extend these studies to two-particle correlations where one particle is an electron from the decay of a heavy-flavor meson and the other is a charged hadron from either the decay of the heavy meson or from jet fragmentation. These measurements provide more detailed information about the interactions between heavy quarks and the matter, such as whether the modification of the away-side-jet shape seen in hadron-hadron correlations is present when the trigger particle is from heavy-meson decay and whether the overall level of away-side-jet suppression is consistent. We statistically subtract correlations of electrons arising from background sources from the inclusive electron-hadron correlations and obtain two-particle azimuthal correlations at $\sqrt{s_{NN}} = 200$ GeV between electrons from heavy-flavor decay with charged hadrons in $p+p$ and also first results in Au+Au collisions. We find the away-side-jet shape and yield to be modified in Au+Au collisions compared to $p+p$ collisions.

I. INTRODUCTION

Experiments at the Relativistic Heavy Ion Collider (RHIC) at Brookhaven National Laboratory have produced a hot dense partonic matter [1,2]. Results from high-p_T π^0 production indicate that fast partons moving through the matter lose a substantial amount of energy through interactions [3,4]. This energy loss was expected to be reduced for heavy charm and bottom quarks due to the dead cone effect which suppresses gluon radiation [5]. However, electrons from the semileptonic decay of D and B mesons are seen to be suppressed at nearly the same level as π^0s out to the highest measured p_T, ≈ 10 GeV/c [6]. This challenges the picture of gluon radiation as the dominant means of parton energy loss. Various alternative scenarios, including collisional energy loss [7], in-medium formation, and dissociation of the heavy meson [8] or an increase in the fraction of heavy quarks carried by baryons [9,10] have been proposed to account for the large suppression.

Single-particle yield measurements provide information on the overall deviation of particle production from $p+p$ expectations. However, the observed high-p_T spectra are thought to be dominated by particles that have lost less than the average amount of energy, either due to a short path length through the matter or by a fluctuation. In order to get more detailed information about the interactions between the

particles and the matter two-particle azimuthal correlations have been extensively used. In $p+p$ collisions these correlations are characterized by two back-to-back jet peaks [11]. At small azimuthal angular difference, $\Delta\phi$, particles are from the fragmentation of the same jet; at $\Delta\phi \approx \pi$ particles are from the fragmentation of partons in the opposing jet.

In heavy-ion collisions, these correlations can provide information about the pattern of energy loss for the back-to-back dijet system as well as other interactions between the fast partons and the medium. Measurements of hadrons associated with a high-p_T hadron have shown the away-side correlations from back to back dijets to be significantly suppressed [12–15]. Measurements of the correlations of electrons from heavy-flavor decay with other hadrons in the event can also provide insight into heavy-flavor energy loss and how this compares to π^0 and direct photon triggered correlations where the modifications could differ due to the different partons probing the matter. This is crucial for building a quantitative understanding of the nature of the interactions between hard partons and the produced hot matter.

In addition, a strong broadening and double peak (shoulder) structure of away-side correlations at moderate p_T has been observed [16]. Many theoretical ideas have been proposed to explain this modification, including Čerenkov gluon radiation [17,18], large-angle gluon radiation [19,20], and Mach shock waves [21]. Measurements of the shoulder structure with particles from the fragmentation of heavy quarks, especially bottom, are interesting because at moderate momenta the quark velocity will be much smaller than the speed of light, in

---

TABLE I. Ratio of heavy-flavor electrons to background electrons in $p+p$ along with the systematic uncertainty.

p_T (GeV/c)	R_{HF}
1.5–2.0	0.66 ± 0.13
2.0–2.5	0.86 ± 0.14
2.5–3.0	1.09 ± 0.14
3.0–3.5	1.31 ± 0.16
3.5–4.0	1.49 ± 0.17
4.0–4.5	1.60 ± 0.17

contrast to light quarks where $v \approx c$ at all jet momenta. In a Mach shock-wave scenario the cone angle of the double peak structure away from π, (θ_M), is related to the speed of the parton by $\cos \theta_M = \frac{c_S}{v}$, where c_S is the speed of sound in the matter and v is the speed of the parton as it propagates through the matter. It has been proposed that double-peaked correlations that do not obey Mach's Law could favor strongly coupled AdS/CFT string drag scenarios [22] or transverse flow [23]. An alternative explanation based on geometrical fluctuations in the initial state leading to triangular flow has also recently been proposed [24–26].

Measurements in $p+p$ collisions are a necessary baseline to heavy-ion measurements, particularly for heavy-flavor triggered correlations. At leading order, several subprocesses contribute to charm production leading to a midrapidity D meson. For $p_T < 10$ GeV/c, one leading-order calculation shows that $\approx 20\%$ of the time the charm quark leading to the D, which decays semileptonically into the trigger electron, is balanced by an opposing $(\Delta\phi \approx \pi)$ $\bar{c}$ quark [27]. The rest of the contribution is from processes such as $cg \to cg$ or $cq(\bar{q}) \to cq(\bar{q})$, where the c is not balanced by a midrapidity, high-p_T $\bar{c}$. Next-to-leading-order effects are known to be large in heavy-quark production. The POWHEG Monte Carlo calculation [28], which includes $2 \to 3$ processes, also shows substantial contributions to the away-side correlations from gluons. Thus, in order to measure $c\bar{c}$ or $b\bar{b}$ correlations, one should identify the heavy quark in both the trigger and away jets. For the present purposes, this means it is not possible to identify the jet opposing the electron from heavy-flavor decay unambiguously as also from heavy-quark fragmentation. This complicates the interpretation of the present measurements. However, the comparison of heavy- and light-flavor-triggered correlations can still provide a crucial

TABLE II. Ratio of heavy-flavor electrons to background electrons in Au+Au along with the systematic uncertainty.

p_T (GeV/c)	R_{HF}
1.5–2.0	0.94 ± 0.21
2.0–2.5	1.14 ± 0.25
2.5–3.0	1.29 ± 0.30
3.0–3.5	1.38 ± 0.34
3.5–4.0	1.43 ± 0.36
4.0–4.5	1.38 ± 0.36

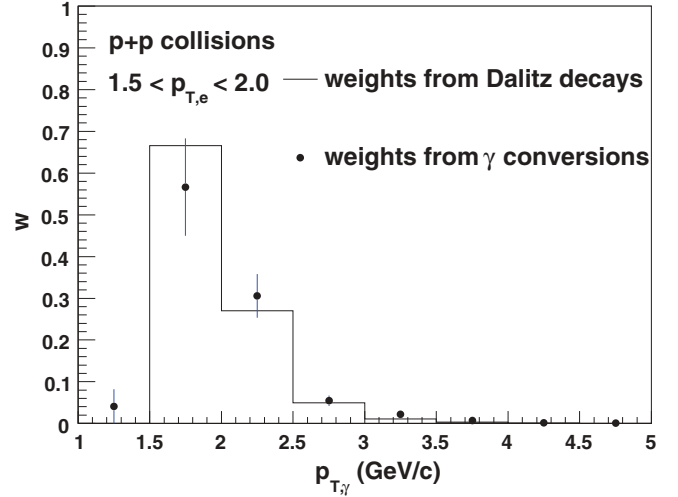

FIG. 1. (Color online) Weights (w) for electrons with $1.5 < p_T < 2.0$ GeV/c from the method using Dalitz decays (histogram) and photon conversions (solid points) as a function of the photon p_T.

step toward understanding fast-parton propagation through the matter.

In the present work heavy-flavor electrons are those from the decay of both D and B mesons. The relative contribution of electrons from bottom to the total heavy-flavor electron yield changes with the p_T of the electron and has been measured in $p+p$ collisions to be from ≈ 10–50% for $1.0 < p_T < 6.0$ GeV/c [29,30]. Fixed-order plus next-to-leading-log (FONLL) calculations from Ref. [31] agree well with the measured bottom contribution.

We present first results of the azimuthal correlations between electrons from the decay of heavy-flavor mesons
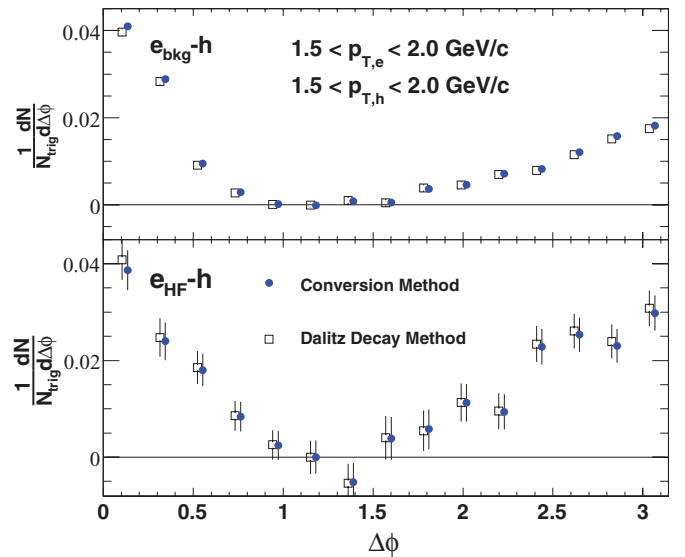

FIG. 2. (Color online) e_{bkg}-h (top panel) and e_{HF}-h (bottom panel) conditional yields for $p+p$ collisions with $1.5 < p_{T,e} < 2.0$ GeV/c and $1.5 < p_{T,h} < 2.0$ GeV/c for the two methods of constructing e_{bkg}-h conditional yields: the conversion method (solid circles) and the Dalitz decay method (black squares). Points have been offset slightly for clarity.
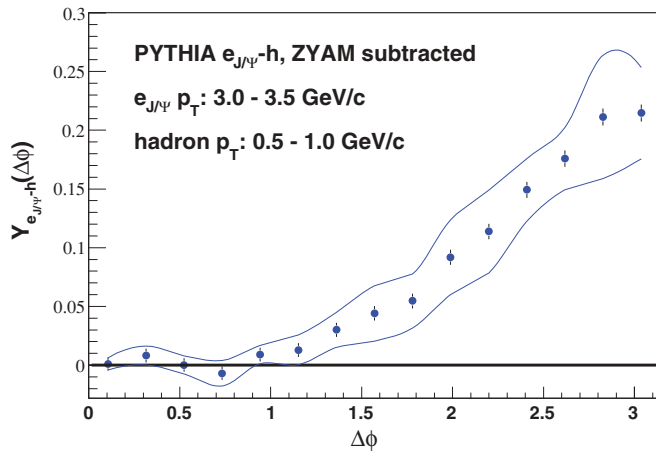
FIG. 3. (Color online) PYTHIA $e_{J/\Psi}$-h correlations after ZYAM subtraction for electrons with $3.0 < p_T < 3.5$ GeV/c and hadrons with $0.5 < p_T < 1.0$ GeV/c. The central values are from the default PYTHIA J/Ψ production setting and the lines show the systematic uncertainty set by the magnitude of the maximal deviation between the default setting at the color singlet and color octet production settings.

with charged hadrons in Au+Au and $p+p$ collisions. We statistically subtract correlations from electrons due to background electron sources (Dalitz decays, photon conversions, and quarkonia) from the measured inclusive electron-hadron correlations.

The paper is organized as follows. In Sec. II we outline the analysis procedure used; in Sec. III we show the results in $p+p$ and Au+Au collisions; and in Sec. IV we conclude and discuss the prospects for future measurements.

II. ANALYSIS METHOD

A. Experimental setup

These results are based on 1.1 billion level-1 triggered $p+p$ events sampling 8.0 pb^{-1} taken during the 2006 RHIC running period and 2.6 billion minimum bias Au+Au events, corresponding to 0.41 nb^{-1} taken during the 2007 RHIC running period. The events were triggered by a hit in each of two beam-beam counters (BBC) at $3.1 < |\eta| < 3.9$ and the interaction is required to be within 25 cm of the center of the interaction region. The $p+p$ level-1 triggered sample also required an energy deposit of approximately 1.4 GeV in an overlapping tile of 4×4 EMCal towers in coincidence with the BBC trigger. EMCal towers are $\Delta\phi \times \Delta\eta \approx 0.01 \times 0.01$. In Au+Au collisions the event centrality is measured by the charge seen in the BBC [32].

The charged-particle tracks and photons used in this analysis are measured in the PHENIX central arm spectrometers. Electrons are measured between 1.5 and 4.5 GeV/c and charged hadrons are measured between 0.5 and 4.5 GeV/c. PHENIX has two such spectrometers, East and West Arms, each covering $\pi/2$ rad in azimuth and $|\eta| < 0.35$. This analysis uses in each arm a drift chamber (DC), two layers of pad chambers (PC1 and PC3), a ring imaging Čerenkov
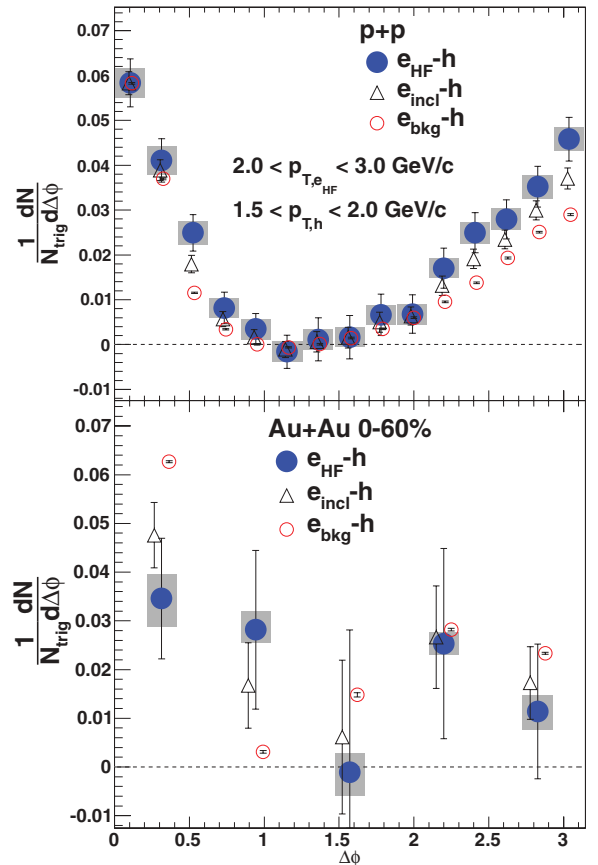

FIG. 4. (Color online) e_{inc}-h, e_{bkg}-h, and e_{HF}-h (solid circles) for $p+p$ (top panel) and Au+Au (bottom panel) collisions for $2.0 < p_{T,e} < 3.0$ GeV/c and $1.5 < p_{T,h} < 2.0$ GeV/c. The overall normalization uncertain of 7.9% in $p+p$ and 9.4% in Au+Au is not shown.

detector (RICH), and an electromagnetic calorimeter (EMCal). Charged particles (both electrons and hadrons) are reconstructed in the DC and PC1. Electron identification is done by requiring two (three) associated hits in the RICH for $p+p$ (Au+Au), a shower-shape cut in the EMCal, and an E/p cut, where E is the energy of the cluster in the EMCal and p is the track momentum determined by the DC. Electron candidates are required to have a matching hit in the EMCal within 3σ (2σ) in $p+p$ (Au+Au). Cuts on the RICH ring center and shape are also included. The hadron contamination remaining is less than 1% in $p+p$ collisions and less than 3% in Au+Au collisions. Hadrons are identified by a RICH veto and a confirming hit in the PC3. Photons are identified by a shower shape cut in the EMCal and a veto in the PC3 to reject charged tracks. Hadron contamination in the photon sample is less than 4%. Cuts on electron-hadron and photon-hadron pairs are also used to equalize the pair acceptance between real and mixed pairs and remove pairs that share hits in the various detector subsystems.

In the Au+Au running period the hadron blind detector (HBD) [33] was installed for a commissioning run between the beam collision vertex position and the central arms. Photon conversions in the detector material were an additional source of background electrons in the inclusive electron
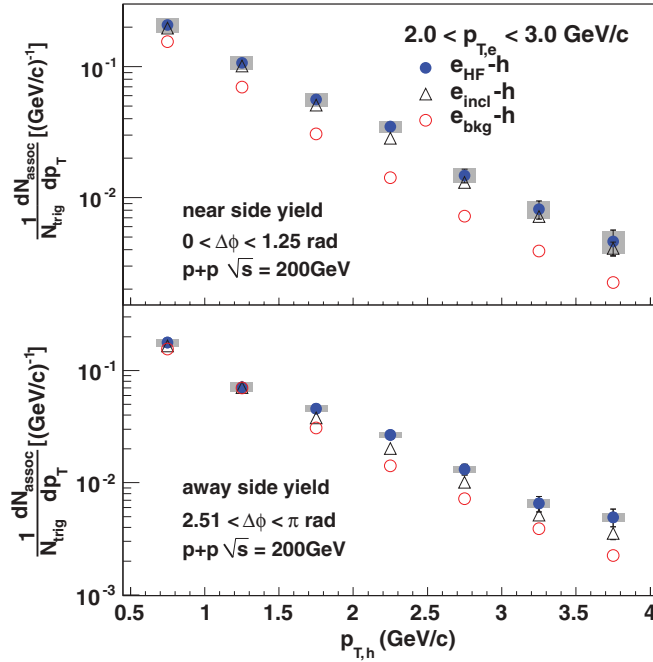
FIG. 5. (Color online)   Near (top) and away (bottom) side conditional yields in $p+p$ collisions as a function of hadron p_T. e_{inc} triggers are shown as triangles, e_{bkg} triggers are shown as open circles, and e_{HF} triggers are shown as solid circles. The boxes on the e_{HF}-h points are the systematic uncertainties except for the overall normalization uncertainty of 7.9%, which is not shown.

sample. The HBD in front of the West Arm was absent for a substantial portion of the running period. We make the additional requirement that electrons from the 2007 running period are reconstructed in the West Arm and select events only from the running period where the HBD in front of the West Arm was removed in order to reduce the number of photon conversions.

B. Background subtraction

In two-particle correlations there is a combinatorial background due to pairs where the particles are uncorrelated except by eventwise correlations, such as centrality and the reaction plane in Au+Au or the underlying event in $p+p$ collisions. This background is very large in central Au+Au collisions and much smaller in $p+p$ collisions. In Au+Au collisions the background is removed by the absolute background subtraction technique [34] while in $p+p$ collisions by the zero yield at minimum (ZYAM) method [35] (with the uncertainties determined as in Ref. [34]) is used to subtract the $\Delta\phi$-independent underlying event. In the absolute background subtraction method the combinatorial background yield is determined from the centrality dependence of the single-particle yields. The principal advantages of this method for this analysis are that the background uncertainty is not subject to statistical fluctuations caused by the small number of electron-hadron pairs and no assumption is made about the shape of the pair $\Delta\phi$ distribution.
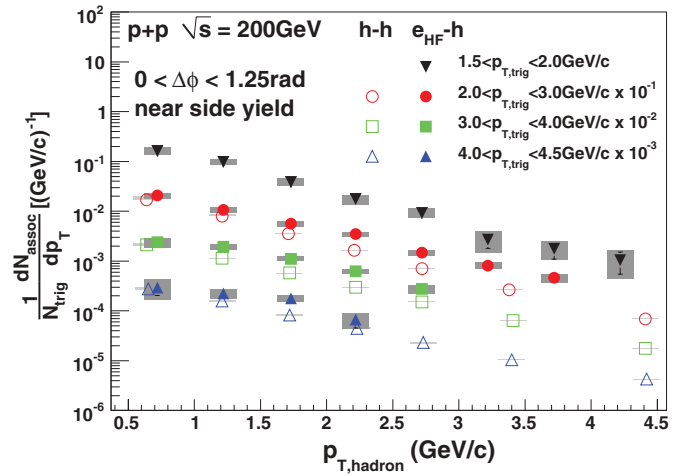
FIG. 6. (Color online) Near-side e_{HF}-h conditional yields in $p+p$ collisions (solid points) as a function of the associated hadron p_T. For comparison hadron-hadron conditional yields in $p+p$ collisions from Ref. [14] are also shown (the $\Delta\phi$ range for the hadron-hadron yields is $\Delta\phi < \pi/3$). The associated hadron p_T spectra are harder for e_{HF}-h than hadron-hadron conditional yields at the same $p_{T,\mathrm{trig}}$ range (the highest p_T trigger selection is for 4.0–4.5 GeV/c for the e_{HF} triggers and 4.0–5.0 GeV/c for the hadron triggers). The overall normalization uncertainty of 7.9% is not shown.

In $p+p$ collisions the underlying event independent of $\Delta\phi$. However, in Au+Au collisions there are additional correlations due to elliptic flow, v_2. These correlations do not affect the magnitude of the combinatorial background but do affect the azimuthal correlation of particles. The v_2 values used in this analysis are measured using the reaction plane as determined from the PHENIX reaction plane detector and the same particle cuts used in the correlation analysis.

Results are reported as conditional yields of hadrons associated with trigger electrons after combinatorial background subtraction, $Y_{e-h}(\Delta\phi)$:

$$Y_{e-h}(\Delta\phi) = \frac{1}{N_e \epsilon_h} \frac{dN_{\mathrm{meas}}}{d\Delta\phi} - B\left[1 + 2v_2^e v_2^h \cos(2\Delta\phi)\right], \quad (1)$$

where N_e is the total number of observed trigger particles and ϵ_h is the reconstruction efficiency for the associated hadrons as determined by a GEANT-based Monte Carlo simulation and embedding single particles into real events. $\frac{dN_{\mathrm{meas}}}{d\Delta\phi}$ is the measured trigger-associated particle $\Delta\phi$ distribution, which has been corrected for nonuniform two-particle $\Delta\phi$ acceptance by using mixed events [34]. B is determined by the background subtraction methods described above.

C. Removal of nonopen heavy-flavor electron-hadron correlations

Studies of electrons from open heavy-flavor decay are complicated by the background of electrons from light meson decay, photon conversions, and, at higher p_T, quarkonia and Drell-Yan. In this analysis we statistically subtract the correlations from these background sources using a method similar to that used to measure direct photon-hadron
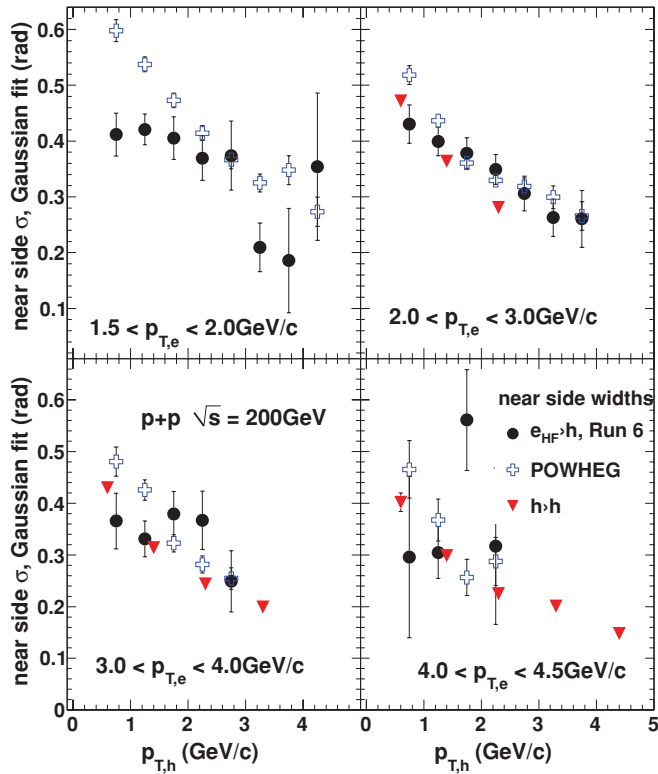
FIG. 7. (Color online) Gaussian widths of near-side conditional yields as a function of the associated hadron p_T for four $p_{T,e}$ selections. Solid circles show results from e_{HF}-h correlations and triangles show results from h-h correlations. Crosses are from POWHEG [28] with charm and bottom combined according to FONLL calculations [31].

correlations [36]. The yield of inclusive electron-hadron pairs per electron trigger, the conditional yield $Y_{e_{inc}-h}(p_{T,e}, p_{T,h}, \Delta\phi)$, is measured. This is a weighted average of the conditional yield of hadrons associated with electrons from heavy-flavor decay and the conditional yield of hadrons associated with electrons from the background sources (the dependencies on p_T and $\Delta\phi$ are omitted hereafter for simplicity):

$$Y_{e_{inc}-h} = \frac{N_{e_{HF}} Y_{e_{HF}-h} + N_{e_{bkg}} Y_{e_{bkg}-h}}{N_{e_{HF}} + N_{e_{bkg}}}, \quad (2)$$

where $N_{e_{HF}}$ ($N_{e_{bkg}}$) is the number of electrons from heavy-flavor decay (background sources). $Y_{e_{HF}-h}$ can then be written as

$$Y_{e_{HF}-h} = \frac{(R_{HF}+1)Y_{e_{inc}-h} - Y_{e_{bkg}-h}}{R_{HF}}, \quad (3)$$

where $R_{HF} \equiv \frac{N_{e_{HF}}}{N_{e_{bkg}}}$. The two quantities to be determined are R_{HF} and $Y_{e_{bkg}-h}$. R_{HF} can be determined by comparing the measured electron yields to the known sources of background electrons. The $Y_{e_{bkg}-h}$ determination is based on measured and simulated azimuthal correlations of the sources of background electrons and is described in detail below.

The R_{HF} value giving the composition of the electron triggers into heavy-flavor and background sources is taken from the published PHENIX measurements [6,37] for the
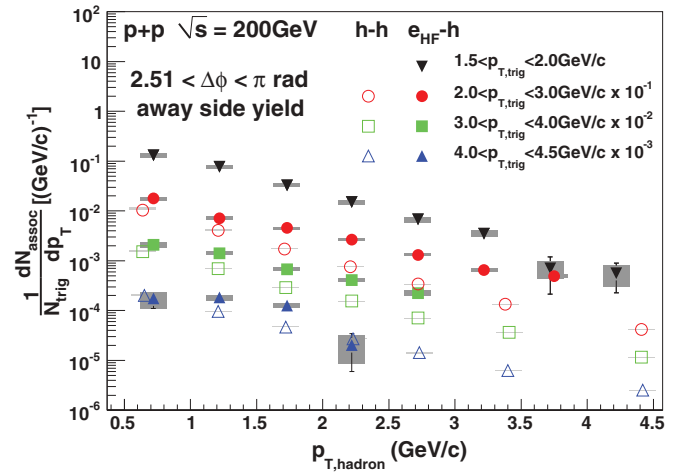
FIG. 8. (Color online) Away-side e_{HF}-h ($2.51 < \Delta\phi < \pi$) conditional yields in $p+p$ collisions (solid points) as a function of the associated hadron p_T. For comparison hadron-hadron conditional yields in $p+p$ collisions from Ref. [14] are also shown (the $\Delta\phi$ range for the hadron-hadron yields is $2.51\Delta\phi < \pi$). The associated hadron p_T spectra are harder for e_{HF}-h than hadron-hadron conditional yields at the same $p_{T,trig}$ range (the highest p_T trigger selection is for 4.0–4.5 GeV/c for the e_{HF} triggers and 4.0–5.0 GeV/c for the hadron triggers). The overall normalization uncertainty of 7.9% is not shown.

electron p_T bins used in this analysis. Based on simulations the R_{HF} has been decreased to account for extra air conversions due to the removal, in both the $p+p$ and Au+Au data samples, of the helium bag, which was installed during the data taking periods of Refs. [6,37]. The removal of the He bag added 0.65% of a radiation length to the material in front of the tracking system. However, the reconstruction efficiency of the electrons from these air conversions decreases with the distance from the interaction point. This was simulated using a GEANT-based description of the PHENIX detector and the electron-identification cuts described above. R_{HF} is reduced by 4.5% in $p+p$ collisions and $\approx$15% in Au+Au collisions
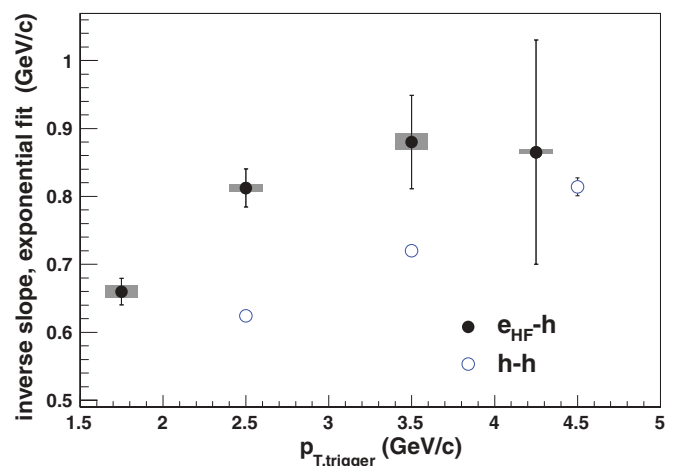

FIG. 9. (Color online) Inverse slope of the e_{HF} triggered away-side conditional hadron p_T distributions shown in Fig. 8 as a function of p_T of the trigger particle. For comparison fits to the hadron-hadron data from Ref. [14] are also shown.

TABLE III. Mean transverse momentum of the parent D and B mesons contributing to the heavy-flavor electron p_T bins used here. They are combined according to the fraction of heavy-flavor electrons from b quarks, $\frac{b \to e}{(c \to e + b \to e)}$ according to the FONLL calculations [31] (as shown in Ref. [29]) to determine the mean heavy-meson transverse momentum.

$p_{T,e}$ (GeV/c)	$\langle p_T \rangle_D$ (GeV/c)	$\langle p_T \rangle_B$ (GeV/c)	$\frac{b \to e}{(c \to e + b \to e)}$	$\langle p_T \rangle_{\text{meson}}$ (GeV/c)
1.5–2.0	3.4	4.4	0.15	3.6
2.0–3.0	4.1	4.7	0.26	4.3
3.0–4.0	5.6	5.6	0.42	5.6

(the reduction is larger in Au+Au collisions, because the magnetic field was configured differently during that period, resulting in increased efficiency for conversion electrons away from the interaction point). Additionally, electrons arising from the decay of quarkonia are a source of background to electrons from semileptonic decay of open heavy-flavor mesons [38], further reducing R_{HF}. The reduction in R_{HF} due to electrons from quarkonia decays is determined by J/Ψ

measurements [39,40] and simulations of the decay (for a more detailed discussion, please see Ref. [38]). The change to the background yield is 3% at $1.5 < p_T < 2.0$ GeV/c and 38% at $4.0 < p_T < 4.5$ GeV/c in $p+p$ collisions. At moderate and high p_T the heavy-flavor signal is larger than the background, so the change to the heavy-flavor electron spectra is much smaller [38]. At all but the highest p_T used here the change is only due to electrons from J/Ψ. Electrons from Υ become
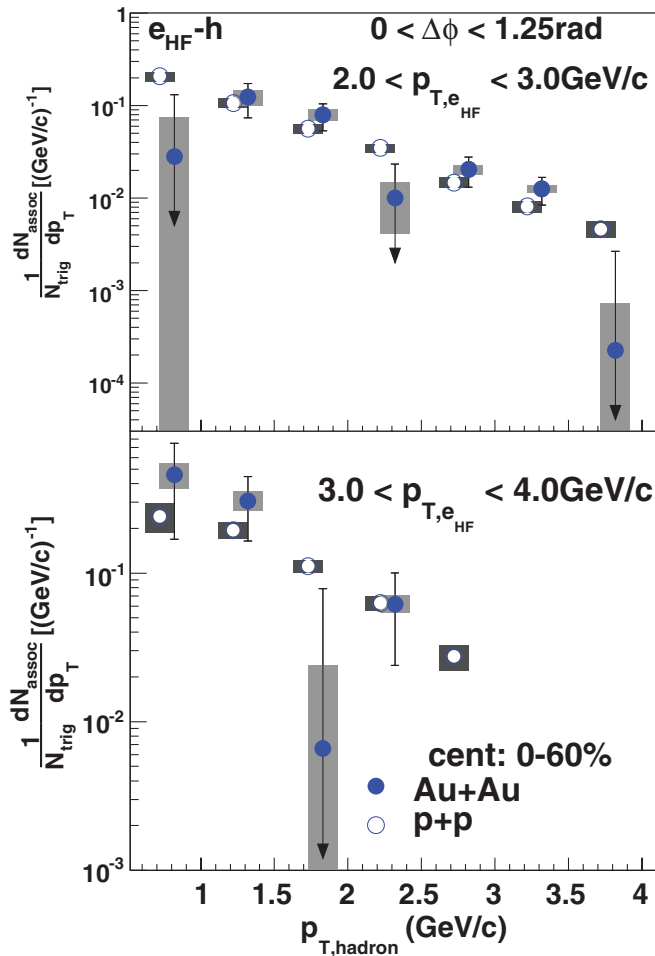
FIG. 10. (Color online) Near-side ($0 < \Delta\phi < 1.25$ rad) integrated yield for Au+Au (solid circles) and $p+p$ collisions (open circles) for $2.0 < p_{T,e} < 3.0$ GeV/c (top panel) and $3.0 < p_{T,e} < 4.0$ GeV/c (bottom panel) as a function of the associated hadron p_T. The overall normalization uncertainty of 9.4% in Au+Au and 7.9% in $p+p$ is not shown. Points are slightly shifted horizontally for clarity.
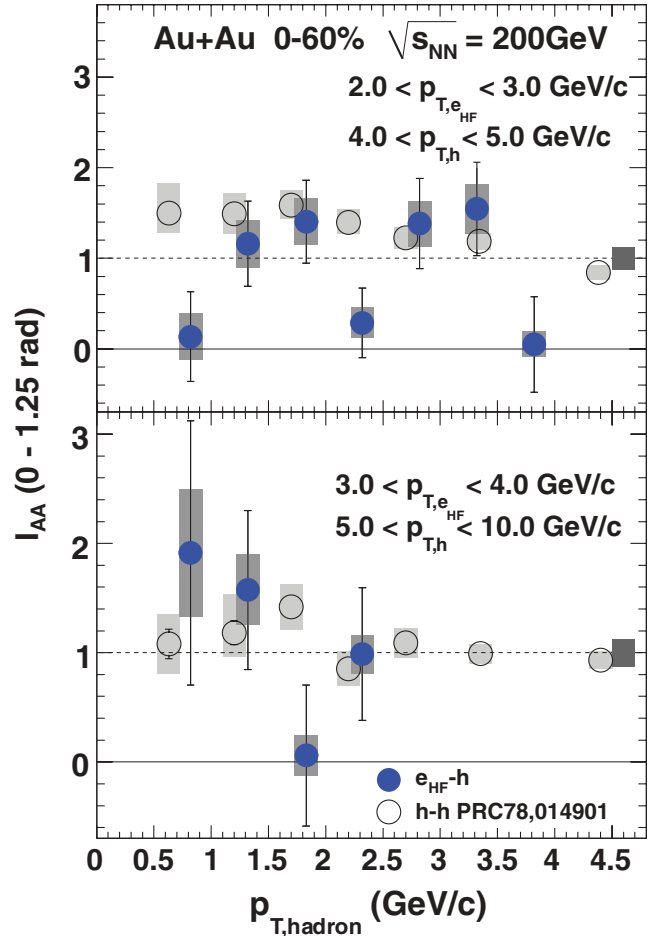

FIG. 11. (Color online) Near-side ($0 < \Delta\phi < 1.25$ rad) I_{AA} for $2.0 < p_{T,e} < 3.0$ GeV/c (top panel) and $3.0 < p_{T,e} < 4.0$ GeV/c (bottom panel) as a function of the associated hadron p_T for e_{HF} (solid points) and hadron (open points) triggers (from Ref. [14]). The gray band around unity shows the overall normalization uncertainty (12.4%), which moves all points together. Points are slightly shifted horizontally for clarity.
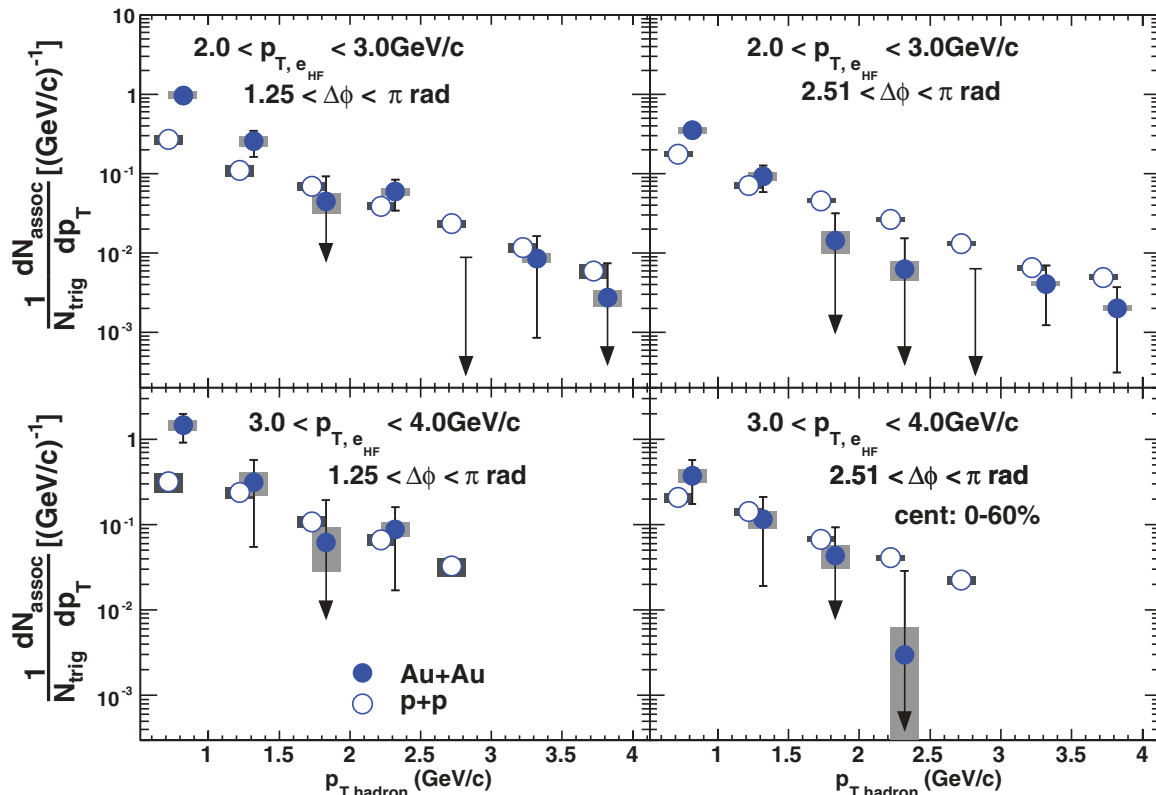
FIG. 12. (Color online) Away-side conditional yields for wide (left) and narrow (right) away-side $\Delta\phi$ integration ranges for Au+Au (solid points) and $p+p$ (open points). Top panels show $2.0 < p_{T,e} < 3.0$ GeV/c and bottom panels shown $3.0 < p_{T,e} < 4.0$ GeV/c. Upper limits are for 90% confidence levels. The overall normalization uncertainty of 9.4% in Au+Au and 7.9% in $p+p$ are not shown. Points are slightly shifted horizontally for clarity.

important at $p_T > 4.0$ GeV/c and electrons from Drell-Yan are negligible at all transverse momenta used in this analysis. The R_{HF} values used in this analysis are shown in Table I ($p+p$) and Table II (Au+Au).

The remaining unknown in Eq. (3) is the azimuthal correlations of the background electrons with hadrons, $Y_{e_{\mathrm{bkg}}-h}$. These pairs can be divided into two classes: those from *photonic* sources (electrons from the decay of light mesons and photon conversions in the detector material) and those from quarkonia (electrons from light vector meson decay are a small contribution and are neglected). These correlations are determined from inclusive photon-hadron correlations. Inclusive photons, like photonic electrons, are largely from π^0 and η decay at $p_T < 5$ GeV/c, and PYTHIA (version 6.421) [41] simulations of the correlations between electrons from J/Ψ decay with hadrons. The fraction of hadrons misidentified as electrons is small, as discussed above, and those correlations are not separately subtracted. At $p_{T,e} < 2$ GeV/c there is a small ($\approx$3%) contribution from electrons from the semileptonic decay of kaons whose correlations are also neglected.

1. Photonic electron correlations

Photonic electron sources include Dalitz decays and photon conversions where the photons are from light meson decay. To

determine these correlations, $Y_{e_{\mathrm{phot}}-h}$, we measure inclusive photon-hadron correlations. Inclusive photons are dominantly also from light meson decay. However, the parent meson p_T distributions need not be the same for photonic electrons and inclusive photons. The relationship can be written as

$$Y_{e_{\mathrm{phot}}-h}(p_{T,i}) = \sum_j w_i(p_{T,j}) Y_{\gamma_{\mathrm{inc}}-h}(p_{T,j}), \qquad (4)$$

where each i (j) represents a 0.5 GeV/c bin in electron (photon) p_T. The weight coefficients $w_i(p_{T,j})$ are determined via simulation and are used to transform the inclusive photon-hadron correlations into expectations for photonic electron-hadron correlations.

Two methods are used to determine the $w_i(p_{T,j})$. The first method treats the electrons as coming from photon conversions in the detector material and the second treats the electrons as coming from Dalitz decays. True photonic electrons come from both sources; however, both methods give very similar $w_i(p_{T,j})$ values.

In the first method the measured single inclusive photon spectrum is input into a GEANT-based simulation of the PHENIX detector. The same electron identification cuts as in the real data analysis are then applied to reconstructed conversion electrons and the relationship between the input photon p_T and the reconstructed conversion electron p_T determines w.
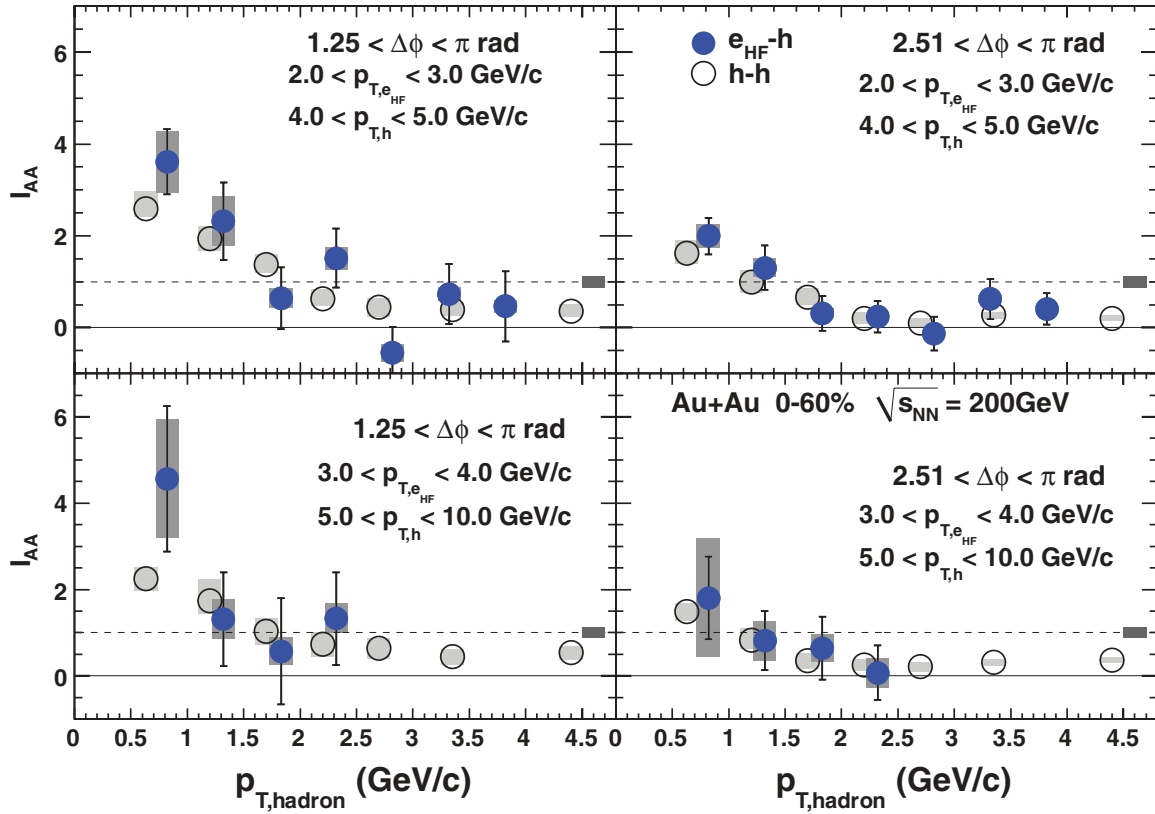
FIG. 13. (Color online) I_{AA} as determined from the away-side yields in Fig. 12. Two $\Delta\phi$ ranges are shown: $1.25 < \Delta\phi < \pi$ rad (left panels) and $2.51 < \Delta\phi < \pi$ rad (right panels). The gray band around unity shows the overall normalization uncertainty of 12.4%, which moves all points together. For comparison hadron-hadron I_{AA} values from Ref. [14] are also shown for trigger p_T selections where the parent heavy meson has similar p_T to the trigger light hadron (see Table III). Points are slightly shifted horizontally for clarity. The solid horizontal line is at 0 and the dashed horizontal line is at 1.

In the second method, the π^0 spectrum from Ref. [42] (for $p+p$ collisions) or Ref. [4] (for Au+Au collisions) is taken as input to a Monte Carlo simulation that decays the π^0s via Dalitz decay. The relationship between the intermediate
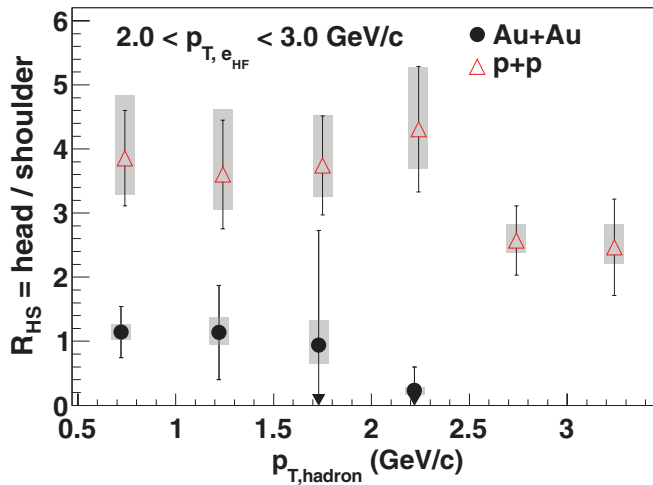

FIG. 14. (Color online) Ratio of the yield in the head region per radian to that in the shoulder region per radian for Au+Au (black) and $p+p$ (red).
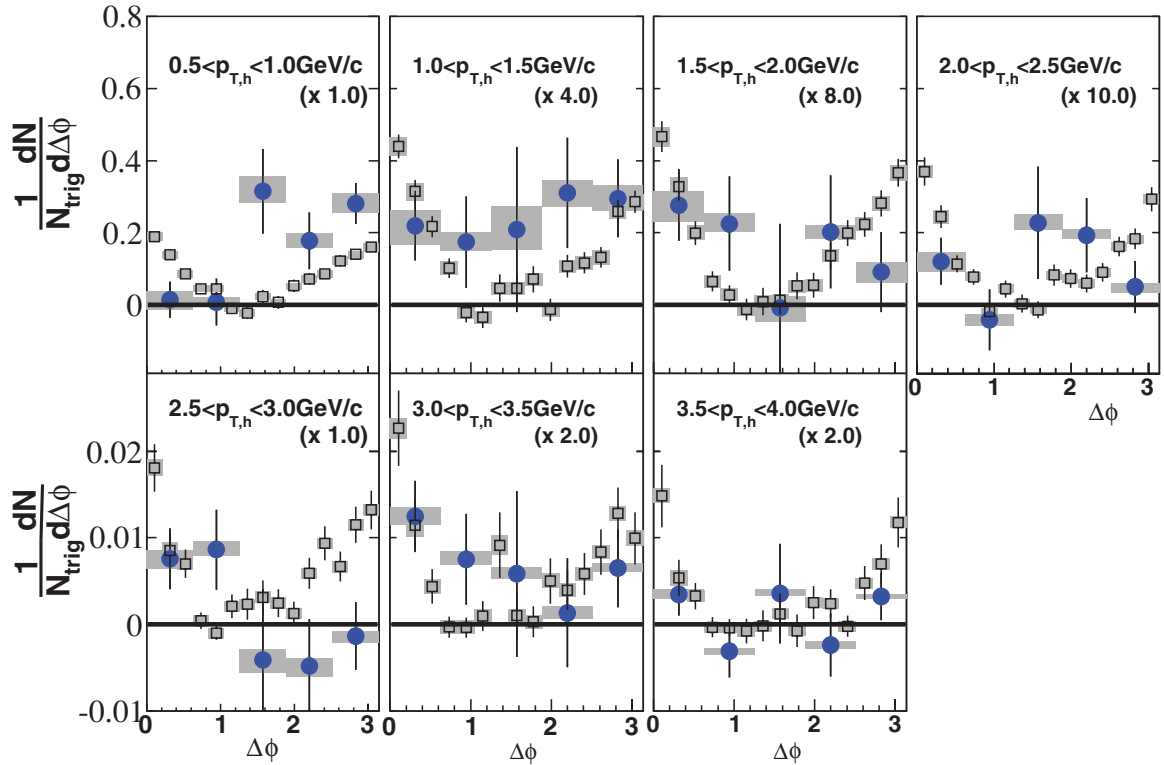
low-mass virtual photon and the resulting decay electron are used in the same manner as in the first method to determine w. Since the mass of the virtual photon is small the difference in the p_T distribution between real photons and the virtual photons in the Dalitz decay is negligible.

Figure 1 compares the w from the two methods for a single electron p_T selection and shows that the differences between the two methods are small. The maximum deviation in the resulting e_{HF}-h conditional yields is at small $\Delta\phi$, where the difference between the two methods is 0.008 (0.006) in $p+p$ (Au+Au). Both inclusive photons and electrons from Dalitz decays are largely the result of π^0 decay. The π^0 spectrum falls steeply with p_T and thus the measured photonic electrons at a given p_T are dominated by those carrying a large fraction of the π^0 p_T regardless of whether the electron comes from a conversion or a Dalitz decay. This argument holds for all heavier mesons that contribute to the photonic electron sample, which explains the small difference between the conversion method (including all mesons that decay into photons) and the Dalitz decay method (including only π^0 decay). Figure 2 shows the difference in the e_{bkg}-h and e_{HF}-h correlations for the two methods. The difference is small compared to the statistical uncertainty and is included in the systematic uncertainty. An additional small systematic uncertainty is included from the statistical uncertainty of the simulations.
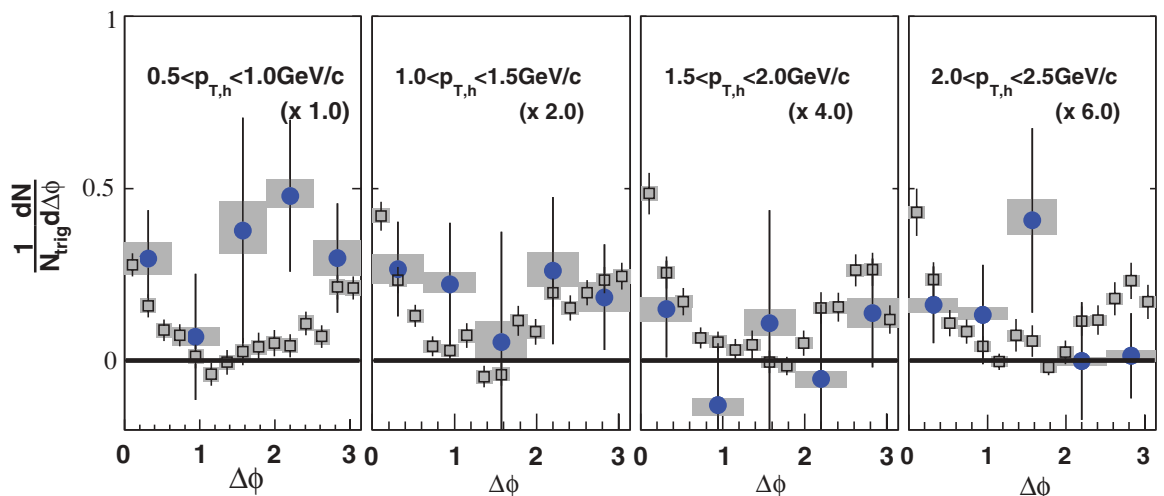
FIG. 15. (Color online) e_{HF}-h jet functions for Au+Au (solid blue circles) and $p+p$ collisions for 2.0–3.0 GeV/c electron triggers and the hadron-p_T bins indicated.

2. Correlations of electrons from quarkonia decay

The azimuthal correlations between J/Ψs and hadrons have not yet been measured at these momenta, so PYTHIA [41] is used to simulate the correlations between the electrons from J/Ψ decay with charged hadrons. For both the Au+Au and $p+p$ measurements the default J/Ψ production within PYTHIA is used. For $p+p$, the systematic uncertainty is taken as the maximal deviation from the default production when varying the production mechanism between color singlet (PYTHIA ISUB = 421) and color octet (PYTHIA ISUB = 422) states. Figure 3 shows the correlations of electrons from J/Ψ decay and hadrons after ZYAM background subtraction for an example p_T selection. For Au+Au, the situation is more uncertain as a substantial fraction of the J/Ψs could be coming from recombining c and $\bar{c}$ quarks [43,44]. In this case, the azimuthal correlations could potentially be strongly reduced;

FIG. 16. (Color online) e_{HF}-h jet functions for Au+Au (solid blue circles) and $p+p$ collisions for 3.0–4.0 GeV/c electron triggers and the hadron-p_T bins indicated.
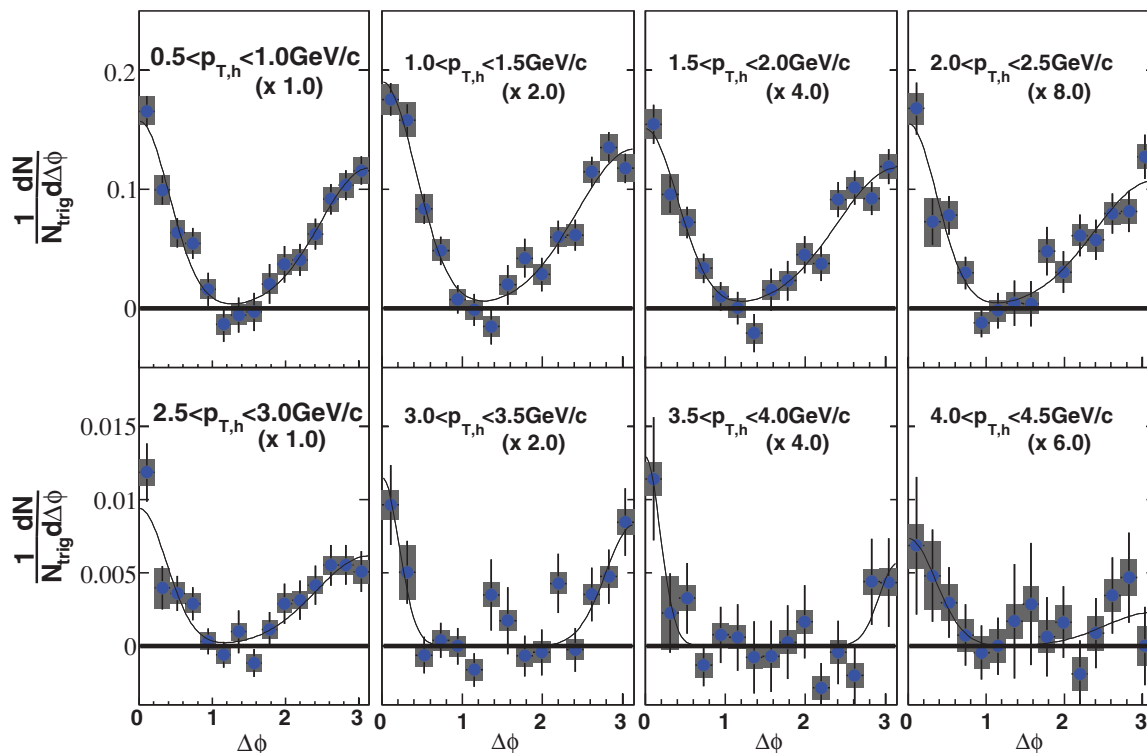
FIG. 17. (Color online) e_{HF}-h jet functions in $p+p$ collisions for 1.5–2.0 GeV/c electron triggers and the hadron-p_T bins indicated.

the systematic uncertainty is taken to extend from the PYTHIA expectation to no correlation between the decay electron and other hadrons.

III. RESULTS AND DISCUSSION

Example jet functions, after efficiency corrections and combinatorial background subtraction, are shown in Fig. 4 for e_{inc}, e_{bkg}, and e_{HF} triggers. Both the near- and away-side jet shapes are clearly present in the $p+p$ data; however, the statistical uncertainties in the Au+Au data are much larger. The boxes show the systematic uncertainties from all sources except for the overall normalization uncertainty of 7.9% in $p+p$ and 9.4% in Au+Au. These jet functions, and others shown in Appendix IV, are integrated and fit to extract the yields and widths that follow. Examples of the integrated near- and away-side conditional yields in $p+p$ collisions are shown in Fig. 5 for the e_{inc}, e_{bkg}, and e_{HF} triggers as a function of the hadron p_T.

A. $p+p$ collisions

The near-side ($0 < \Delta\phi < 1.25$ rad) conditional yields of hadrons associated with heavy-flavor electrons are shown in Fig. 6 for the four electron p_T selections used in this analysis. While, in general, parton fragmentation favors the production of hadrons carrying a small fraction of the parent quark momentum, the heavy meson, D or B, resulting from a heavy-quark fragmentation typically carries a large fraction of the heavy-quark momentum ($z = \frac{p_{hadron}}{p_{jet}}$ is peaked at ≈ 0.60

for charm and ≈ 0.85 for bottom) [45–49]. For comparison we also show the conditional yields from correlations between two charged hadrons from Ref. [14]. The spectra of near-side associated hadrons is harder for the e_{HF} triggers than for the hadron triggers in all overlapping $p_{T,trig}$ selections. The near-side correlations are expected to be dominated by hadrons that are also from the decay of the heavy meson. The large mass of the heavy meson translates to a wider expected near-side correlation when the hadron and the electron are both from the heavy-meson decay. Figure 7 shows the Gaussian widths of the near-side conditional yields as a function of the associated hadron p_T. Also shown for comparison are the near-side widths for hadron-hadron correlations [14], which primarily come from light parton jets. The widths of the e_{HF}-h correlations are slightly wider for $2.0 < e_{HF} < 3.0$ GeV/c, consistent with the near side being dominated by decay-induced correlations. For higher-p_T electrons the statistical uncertainties become too large to make a quantitative statement. Results from POWHEG [28], a next-to-leading-order Monte Carlo calculation, with charm and bottom contributions set by FONLL calculations [31] are shown. These simulations are consistent with the data except for the lowest electron and hadron momenta.

The away-side (summed over $2.51 < \Delta\phi < \pi$ rad) conditional yields are shown in Fig. 8. The yields on the away side are dominated by the fragmentation and decay of particles in the opposing jet. As discussed above the opposing dijet does not have to contain a balancing heavy-flavor quark; here the yields are a mix of heavy and light parton jets. At a given p_T trigger bin the heavy-flavor electron triggered away-side spectrum is harder than the light hadron triggered one. In order
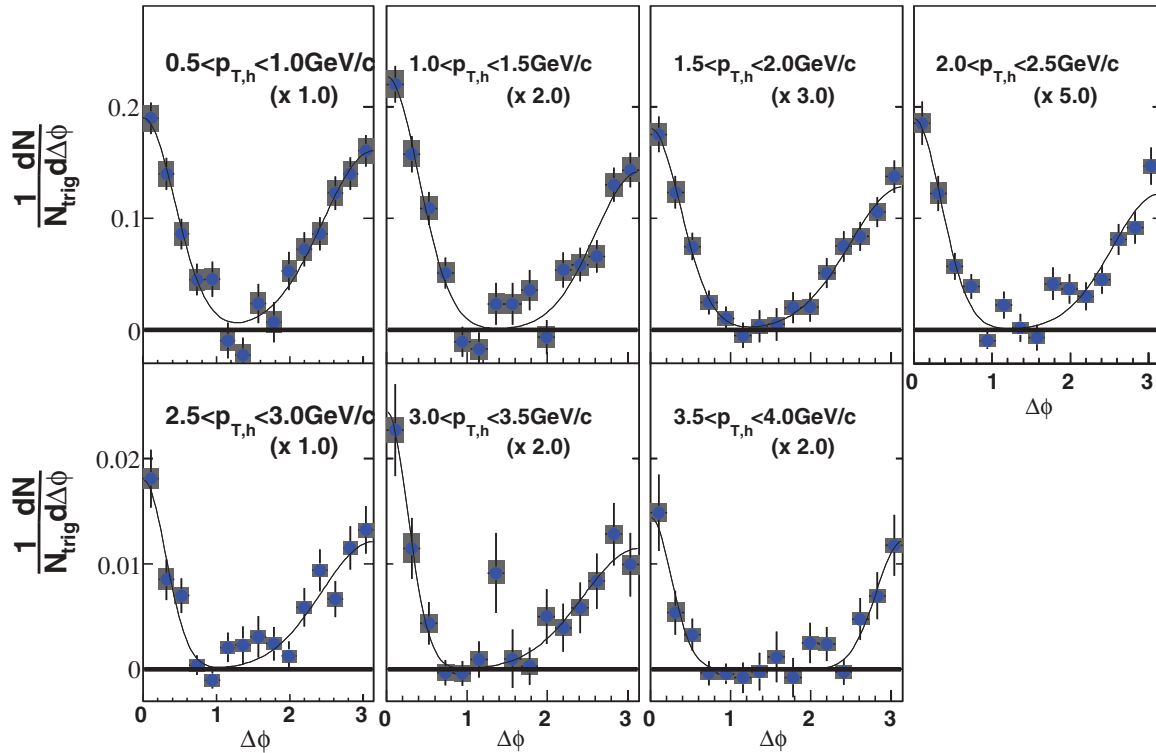
FIG. 18. (Color online) e_{HF}-h jet functions in $p+p$ collisions for 2.0–3.0 GeV/c electron triggers and the hadron-p_T bins indicated.

to quantify the slope differences between light hadron triggers and heavy-flavor electron triggers we plot the inverse slope from an exponential fit of the away-side spectra in Fig. 9.

However, the electron only carries a fraction of the heavy meson p_T. PYTHIA was used to estimate the parent meson average p_T for both charm and bottom mesons and the results are shown in Table III. When comparing the inverse slopes at similar meson p_T, as opposed to similar trigger particle p_T, the difference in the inverse slopes between the two trigger types largely disappears.

B. Au+Au collisions

The conditional yields for the near-side $(0 < \Delta\phi < 1.25$ rad) for Au+Au collisions are compared to $p+p$ collisions in Fig. 10 for Au+Au collisions with 0–60% centrality. In addition, to provide a more direct comparison of the Au+Au and $p+p$ conditional yields we construct the ratio of the conditional yield in Au+Au to $p+p$:

$$I_{\mathrm{AA}} \equiv \frac{\int Y_{e_{\mathrm{HF}}-h}^{\mathrm{AuAu}}(\Delta\phi)d\Delta\phi}{\int Y_{e_{\mathrm{HF}}-h}^{pp}(\Delta\phi)d\Delta\phi} \qquad (5)$$

shown in Fig. 11. In the absence of any nuclear effects I_{AA} will be unity. The near-side I_{AA} is consistent with one $(\chi^2/\mathrm{DOF} = 12.3/7$, statistical uncertainties only). Naively, this might be expected since the near-side correlations in both $p+p$ and Au+Au collisions are expected to largely be from the heavy-meson decay. Since the decay length is long compared to the size and lifetime of the matter produced in Au+Au collisions the subsequent decay of the heavy meson should be

unmodified by the matter. However, it is possible that the charm and bottom contributions are altered from $p+p$ collisions due to medium effects (such as different energy loss for charm and bottom quarks). Additionally, the measured hadrons are not solely from D and B decay, but also from the fragmentation of the heavy quarks and, possibly, from interactions between the heavy quark and the matter. Rather than attempt to disentangle these contributions (which would be highly model dependent) we leave it to theoretical models to reproduce the I_{AA} with the combined hadron sources.

We compare the e_{HF}-h I_{AA} values to those from hadron-hadron collisions at approximately the same meson p_T (see Table III). In hadron-hadron correlations the observed I_{AA} has a strong dependence on the p_T of the trigger hadron [14]. For $2 < p_T < 3$ GeV/c electrons the closest hadron p_T selection from Ref. [14] was $4 < p_T < 5$ GeV/c and for $3 < p_T < 4$ GeV/c electrons it was $5 < p_T < 10$ GeV/c (see Table III). We observe the near-side I_{AA} for heavy-flavor electron triggers to be consistent with those from the comparison hadron triggered results, though the present uncertainties are too large to be sensitive to the excess seen in the hadron-hadron correlations.

In order to be sensitive to possible modifications of the away-side jet shape, we measure the away-side yields in two $\Delta\phi$ ranges as shown in Fig. 12 for e_{HF} triggers with $2.0 < p_{T,e} < 3.0$ GeV/c and $3.0 < p_{T,e} < 4.0$ GeV/c. The wide away-side range, $1.25 < \Delta\phi < \pi$ rad is sensitive to the entire modified away-side shape and the smaller away-side range, $2.51 < \Delta\phi < \pi$ rad, is sensitive to only the $p+p$ like part of the away-side correlations. The ratio of conditional yields in Au+Au to $p+p$ for both away-side $\Delta\phi$ ranges is shown in
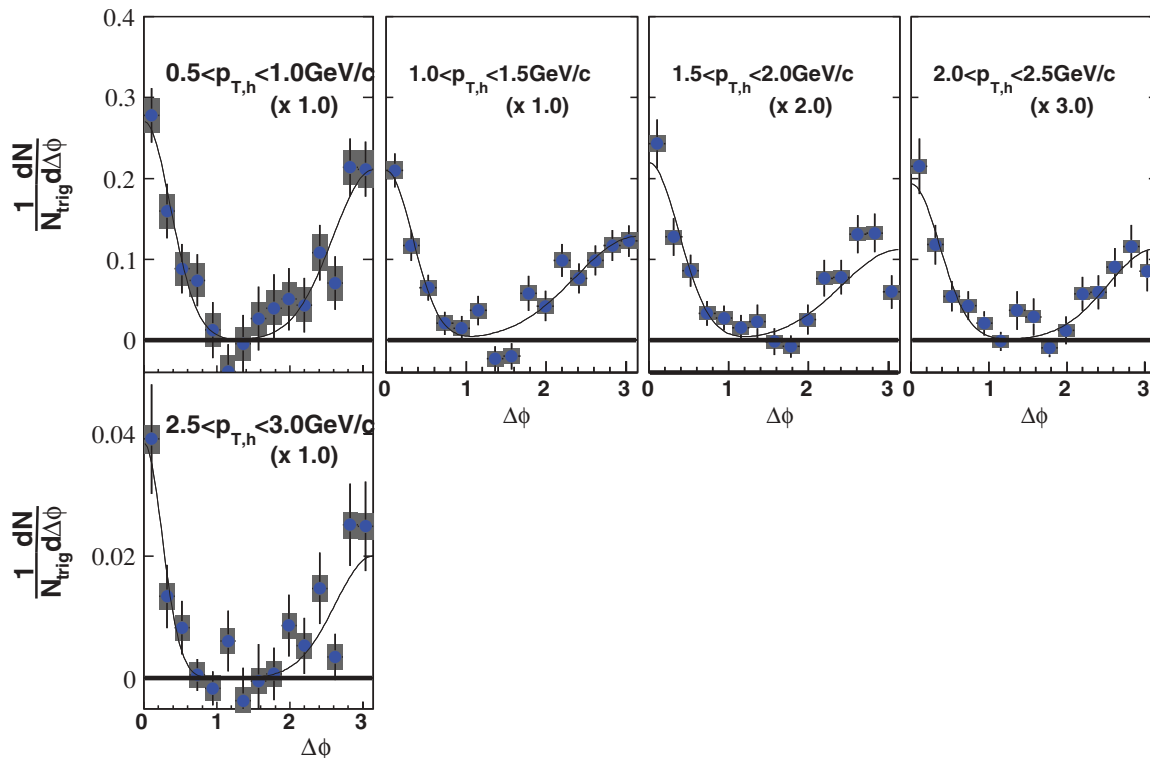
FIG. 19. (Color online) e_{HF}-h jet functions in $p+p$ collisions for 3.0–4.0 GeV/c electron triggers and the hadron-p_T bins indicated.

Fig. 13. I_{AA} is largest at low-hadron p_T and decreases with increasing hadron p_T. For comparison, the hadron-hadron I_{AA} from Ref. [14] is shown for the most closely matched meson p_T selections (see Table III). The heavy-flavor electron triggered I_{AA} is consistent with the hadron-hadron I_{AA} when compared at similar meson p_T selections.

This similarity could be due to the expected large fraction of gluons in the away-side distributions. If the away-side parton path lengths through the matter are similar between heavy-flavor electron and light hadron triggers then the corresponding I_{AA} values should also be similar. However, some fraction of the away-side correlations should be due to correlated heavy-flavor quarks. This can be isolated in future measurements by triggering on back-to-back heavy-flavor electrons. We conclude that the present measurements are not sensitive to any differences caused by back-to-back heavy-flavor pairs, either because the differences between away-side heavy-flavor electrons and light partons are small or because there are too few of them to significantly alter the I_{AA} values.

Motivated by hadron-hadron correlations, we compared the away-side jet shape between $p+p$ and Au+Au collisions. To quantify the shape differences we construct R_{HS} [14], which is the yield per radian in the head region where the $p+p$ jet is peaked (here $2.51 < \Delta\phi < \pi$ rad) divided by the yield per radian in the shoulder region where the enhancement in the Au+Au jet yield is observed in hadron-hadron correlations ($1.25 < \Delta\phi < 2.51$ rad). The systematic uncertainties on the ratio are largely correlated between the head and shoulder region except for the uncertainty due to v_2 in Au+Au

collisions, which is anticorrelated because of the shape of the azimuthal modulation from v_2. In $p+p$ collisions this ratio is large since the yield in the head region is much larger than the yield in the shoulder region. In hadron-hadron correlations for Au+Au collisions R_{HS} is observed to be smaller than in $p+p$ collisions because of the increased yield in the shoulder region [14]. Figure 14 shows R_{HS} for e_{HF}-h correlations for $2.0 < p_{T,e} < 3.0$ GeV/c as a function of the p_T of the associated hadron. R_{HS} is smaller for Au+Au collisions than for $p+p$ collisions indicating that a similar away-side shape modification takes place for e_{HF} triggers as for hadron triggers (the head and shoulder $\Delta\phi$ regions are slightly different between this analysis and Ref. [14] preventing a direct comparison). No $p_{T,h}$ dependence of R_{HS} is observed; however, the statistical uncertainties are quite large.

IV. CONCLUSIONS

Studies of the yields of electrons from the decay of heavy-flavor mesons in Au+Au collisions have challenged the picture of medium-induced radiative energy loss as the dominant mechanism by which high-p_T hadrons are suppressed. Correlations of hadrons from light quark and gluon jets have shown large modifications of the correlation patterns between $p+p$ and Au+Au collisions. Studying the correlations of electrons from the decay of heavy mesons with other hadrons in the event provides more information about how the charm and bottom quarks propagate through the matter and how the modified correlation structures observed in hadron-hadron correlations
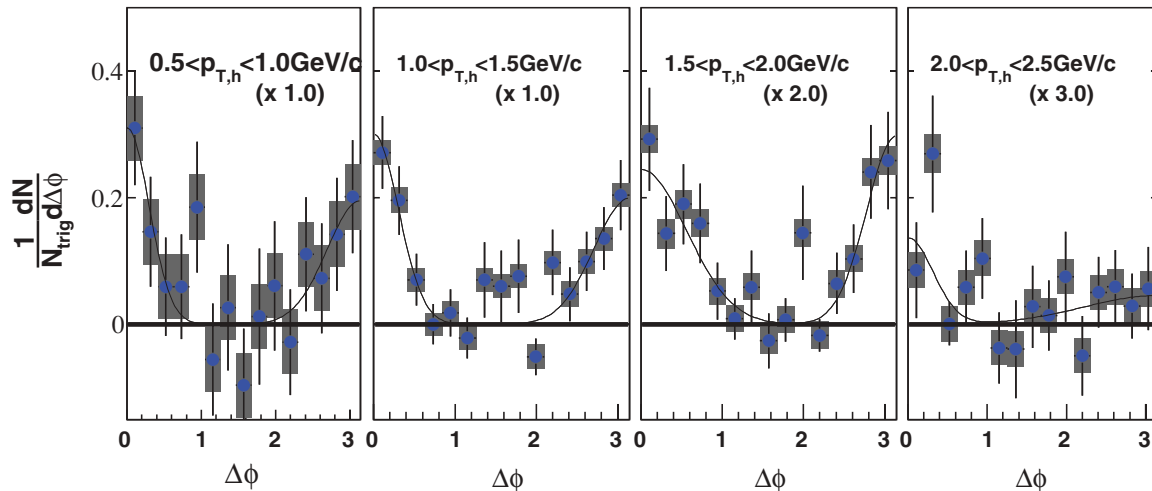
FIG. 20. (Color online) e_{HF}-h jet functions in $p+p$ collisions for 4.0–4.5 GeV/c electron triggers and the hadron-p_T bins indicated.

are produced. Thus, they are a crucial component of hard physics in relativistic heavy-ion collisions. The interpretation is complicated by the ambiguity in the away-side flavor and because the electron does not carry all of the parent meson's momentum. This makes understanding $p+p$ collisions as a baseline very important.

We have presented first measurements of the azimuthal correlations of electrons from heavy-flavor decay with hadrons in both $p+p$ and Au+Au collisions. These measurements provide a first step in understanding correlations involving open heavy flavor in the hot matter produced in heavy-ion collisions. The Gaussian widths of these correlations are consistent with expectations from simulations of the fragmentation of heavy quarks and the decay of heavy-flavor mesons, except for the lowest-p_T electrons and hadrons where some differences are observed. In $p+p$ collisions the spectra of associated hadrons on both the near and away side are harder than in hadron-hadron correlations measured in the same trigger p_T range. However, the level of away-side suppression at large p_T is consistent between electron and hadron triggers when the trigger charged hadron and the parent heavy meson are at approximately the same p_T. The ratio of yields in the head region to those in the shoulder region decreases from $p+p$ to Au+Au collisions in a manner qualitatively consistent with hadron-hadron collisions [14]. Further measurements sensitive to the partonic content of the away-side jets (heavy quarks or light quarks and gluons) are necessary to determine if this is due primarily to cases where the away-side parton is a light quark or gluon or if the suppression of away-side heavy-jet fragmentation is similar to those of light partons.

Near future measurements of heavy-flavor triggered azimuthal correlations hold particular promise. Data taken in 2010 has improved statistics and the HBD was successfully operated allowing the rejection of some of the Dalitz and conversion electron background. Additionally, $d+$Au data taken by PHENIX in 2008 will help constrain any cold nuclear matter effects. Such effects are expected to be small

at midrapidity but are not well constrained by existing data. In future data taking, the silicon vertex detector will be installed, which will enable the separation of electrons from D and B decay and increase acceptance for measuring charged hadrons. Application of the techniques developed here on data taken with these upgrades in place will allow for more detailed heavy-flavor correlation measurements.

APPENDIX: JET FUNCTIONS

Figures 15 and 16 show comparisons of e_{HF}-h jet functions for Au+Au and $p+p$ collisions for the indicated electron triggers and hadron-p_T bins. Figures 17–20 show the e_{HF}-h jet functions for $p+p$ collisions only for the indicated electron triggers and hadron-p_T bins.

[1] K. Adcox *et al.*, Nucl. Phys. A **757**, 184 (2005).
[2] A. Adare *et al.*, Phys. Rev. Lett. **104**, 132301 (2010).
[3] K. Adcox *et al.*, Phys. Rev. Lett. **88**, 022301 (2002).
[4] A. Adare *et al.*, Phys. Rev. Lett **101**, 232301 (2008).
[5] Y. L. Dokshitzer and D. E. Kharzeev, Phys. Lett. B **519**, 199 (2001).
[6] A. Adare *et al.*, Phys. Rev. Lett. **98**, 172301 (2007).
[7] M. Djordjevic, Phys. Rev. C **74**, 064907 (2006).
[8] A. Adil and I. Vitev, Phys. Lett. B **649**, 139 (2007).
[9] P. R. Sorensen and X. Dong, Phys. Rev. C **74**, 024902 (2006).
[10] G. Martinez-Garcia, S. Gadrat, and P. Corchet, Phys. Lett. B **663**, 55 (2008).
[11] S. S. Adler *et al.* (PHENIX Collaboration), Phys. Rev. D **74**, 072002 (2006).
[12] C. Adler *et al.* (STAR Collaboration), Phys. Rev. Lett. **90**, 082302 (2003).
[13] C. Adler *et al.* (STAR Collaboration), Phys. Rev. Lett. **97**, 162301 (2006), arXiv:nucl-ex/0604018.
[14] A. Adare *et al.*, Phys. Rev. C **78**, 014901 (2008).
[15] A. Adare *et al.*, Phys. Rev. Lett. **104**, 252301 (2010).
[16] S. S. Adler *et al.* (PHENIX Collaboration), Phys. Rev. Lett. **97**, 052301 (2006).
[17] I. Dremin, JETP Lett. **30**, 140 (1979).
[18] V. Koch, A. Majumder, and X. N. Wang, Phys. Rev. Lett. **96**, 172302 (2006).
[19] I. Vitev, Phys. Lett. B **630**, 78 (2005).
[20] A. D. Polosa and C. A. Salgado, Phys. Rev. C **75**, 041901 (2007).
[21] J. Casalderrey-Solana, E. V. Shuryak, and D. Teaney, J. Phys. Conf. Ser. **27**, 22 (2005).
[22] B. Betz, M. Gyulassy, J. Noronha, and G. Torrieri, Phys. Lett. B **675**, 340 (2009).
[23] B. Betz, J. Noronha, G. Torrieri, M. Gyulassy, and D. H. Rischke, Phys. Rev. Lett. **105**, 222301 (2011).
[24] J. Takahashi *et al.*, Phys. Rev. Lett. **103**, 242301 (2009).
[25] P. Sorensen, J. Phys. G **37**, 094011 (2010).
[26] B. Alver and G. Roland, Phys. Rev. C **81**, 054905 (2010).
[27] I. Vitev, T. Goldman, M. B. Johnson, and J. W. Qiu, Phys. Rev. D **74**, 054010 (2006).
[28] S. Frixione, P. Nason, and G. Ridolfi, J. High Energy Phys. 09 (2007) 126.
[29] A. Adare *et al.*, Phys. Rev. Lett. **103**, 082002 (2009).
[30] M. M. Aggarwal *et al.*, Phys. Rev. Lett. **105**, 202301 (2010).
[31] M. Cacciari, P. Nason, and R. Vogt, Phys. Rev. Lett. **95**, 122001 (2005).
[32] M. Allen *et al.*, Nucl. Instrum. Methods A **499**, 549 (2003).
[33] Z. Fraenkel *et al.*, Nucl. Instrum. Methods A **546**, 466 (2005).
[34] A. Sickles, M. P. McCumber, and A. Adare, Phys. Rev. C **81**, 014908 (2010).
[35] N. N. Ajitanand *et al.*, Phys. Rev. C **72**, 011902 (2005).
[36] A. Adare *et al.*, Phys. Rev. C **80**, 024908 (2009).
[37] A. Adare *et al.*, Phys. Rev. Lett. **97**, 252002 (2006).
[38] A. Adare *et al.* (PHENIX Collaboration), arXiv:1005.1627 (to be published).
[39] A. Adare *et al.*, Phys. Rev. Lett. **98**, 232002 (2007).
[40] A. Adare *et al.*, Phys. Rev. Lett. **98**, 232301 (2007).
[41] T. Sjoestrand *et al.*, Comp. Phys. Comm **135**, 238 (2001).
[42] S. S. Adler *et al.* (PHENIX Collaboration), Phys. Rev. Lett. **91**, 241803 (2003).
[43] P. Braun-Munzinger and J. Stachel, Phys. Lett. B **490**, 196 (2000).
[44] R. L. Thews, M. Schroedter, and J. Rafelski, Phys. Rev. C **63**, 054905 (2001).
[45] M. Artuso *et al.*, Phys. Rev. D **70**, 112001 (2004).
[46] R. Seuster *et al.*, Phys. Rev. D **73**, 032002 (2006).
[47] A. Heister *et al.*, Phys. Lett. B **512**, 30 (2001).
[48] G. Abbiendi *et al.*, Eur. Phys. J. C **29**, 463 (2003).
[49] K. Abe *et al.*, Phys. Rev. D **65**, 092006 (2002).